Letters in Applied NanoBioScience
Open-Access Journal (ISSN: 2284-6808)

Article
Volume 15, Issue 1, 2026, 36
https://doi.org/10.33263/LIANBS151.036

From Design to Therapy: Chlorolan-1-ylium's Efficacy as a LAP1 Protein Inhibitor in Melanomas

Irfan N [1], Mohammed Zaidh S [2,3*], Mohammad Habeeb [1,*]

[1] Crescent School of Pharmacy, BS Abdur Rahman Crescent Institute of Science and Technology, India
[2] Application Scientist, D3 Drug Tech Lab Pvt Ltd, India
[3] Department of Pharmaceutical Chemistry, SRM College of Pharmacy, SRM Institute of Science and Technology, Kattankulathur, Chengalpattu, Tamil Nadu-603203, India
* Correspondence: ms3597@srmist.edu.in;

Received: 24.10.2024; Accepted: 24.02.2026; Published: 30.03.2026

Abstract: Skin cancer, one of the most prevalent malignancies worldwide, continues to present significant therapeutic challenges, with metastatic melanoma exhibiting a survival rate below 20%. In this study, we investigated the inner nuclear membrane protein LAP1, specifically the LAP1C isoform, as a novel therapeutic target in melanoma. We designed and screened 74 chlorolan-1-ylium derivatives against LAP1 (PDB ID: 4TVS) using structure-based molecular docking, ADMET prediction, molecular dynamics (MD) simulation, and density functional theory (DFT) analysis. The top compound achieved a Glide docking score of –7.456 kcal/mol and an MMGBSA binding free energy of –53.4 kcal/mol, forming stable π-cation, hydrogen bonding, and hydrophobic interactions. A 100 ns MD simulation confirmed structural stability (RMSD ~2.0 Å; RMSF <4.8 Å), and DFT calculations (HOMO –0.8187 eV, LUMO –0.7850 eV, ΔE = 0.0337 eV) suggested high chemical reactivity. Compared with current melanoma therapeutics, this is the first report to propose LAP1 inhibition via chlorolan-1-ylium derivatives, offering a distinct mechanism via laminopathic pathway disruption.

Keywords: genomic analysis; molecular docking; molecular dynamics simulation; ADMET.

1. Introduction

At present, skin cancer poses a public health challenge globally and is the most common cancer. Melanoma is caused by undesirable proliferation in human melanocytes [1]. In the U.S., more than 9500 people are diagnosed every day, two people die every hour, and more than 186,000 new cases occur every year. The exact cause of melanomas is unknown, but UV radiation or high sunlight exposure increases the risk of melanomas [1–3]. The 10 years survival rate of patients with metastatic melanoma has less than 10% having the role of Surgery and Radiation therapy, although using single-agent chemotherapy is well tolerated with a response rate of only 5 to 10%, and those using combinational chemotherapy and bio chemotherapy like FDA approved current drugs in the market like aldesleukin, Binimetinib has greater toxicity not improved survival rate. The radiation treatment for symptomatic metastases may be clinically beneficial for patients, melanoma has been shown to be an extremely radioresistant tumour (Table 1) [3,4]. Cancer cells spread from a primary tumor through metastasis, colonizing other areas. To successfully navigate the physical constraints imposed

by the tissue structure and microenvironment, the mechanical characteristics of the nucleus must be modified during this process [5–9].

Literature has revealed that metastatic melanoma cells, as well as the invasive front of primary melanoma tumors in humans and metastases, express higher levels of the inner nuclear membrane protein LAP1. LAP1B and LAP1C are two isoforms of LAP1 expressed in human cells, distinguished by their different amino termini. Our report indicates that the expression of the shorter isoform, LAP1C, promotes nuclear envelope blebbing, restricts migration and invasion by diminishing the coupling between nuclear and extracellular signals associated with melanoma aggressiveness, thereby making the nucleus more adaptable [9–13]. They hypothesize that LAP1 blocks the signaling laminopathic pathway and that mutations are mainly used to identify the best lead molecule.

Table 1. Comparison of current therapeutic strategies for melanoma with the proposed LAP1.

Therapeutic strategy	Example drug(s)	Primary target	Mechanism of action	Limitations	Our Proposed LAP1 Inhibitor
BRAF inhibitors	Vemurafenib, Dabrafenib	Mutated BRAF V600E	Inhibits MAPK pathway signaling by blocking mutant BRAF kinase activity	Rapid resistance due to MAPK pathway reactivation; limited efficacy in non-BRAF mutants	Targets the LAP1 protein (inner nuclear membrane), disrupting laminopathic pathways associated with metastatic potential
MEK inhibitors	Trametinib, Binimetinib	MEK1/2 kinases	Blocks downstream ERK signaling in the MAPK pathway	Toxicity; limited survival benefit in monotherapy	Novel target unrelated to the MAPK pathway, with potential to bypass existing resistance mechanisms
Immune checkpoint inhibitors	Pembrolizumab, Nivolumab	PD-1 receptor	Restores T-cell-mediated anti-tumor immunity	Immune-related adverse events; non-responsive patient subsets	Small-molecule approach; may be used in combination with immunotherapy for synergistic effects
Cytotoxic chemotherapy	Dacarbazine, Temozolomide	DNA	DNA alkylation leading to apoptosis	Low response rate; high systemic toxicity	Predicted low toxicity profile (ADMET), high selectivity for LAP1 over normal proteins
Our proposed LAP1 inhibitor	—	LAP1C isoform	Blocks nuclear envelope remodeling and signaling, impairing metastatic cell migration/invasion	—	-

While LAP1 overexpression has been implicated in melanoma progression, no small-molecule inhibitors have been reported to date. Current melanoma therapeutics primarily target BRAF and MEK pathways, with limited efficacy in LAP1-associated disease states. This knowledge gap highlights the need for rational drug design strategies targeting LAP1, particularly the LAP1C isoform linked to nuclear adaptability and metastatic potential. Our approach integrates deep learning-based cavity detection, cheminformatics-driven ligand generation, and multi-level computational validation to identify and evaluate novel LAP1 inhibitors, providing a first-in-class strategy against this target.

2. Materials and Methods

The process begins with the retrieval and preparation of the LAP1 protein structure from structural databases. Subsequently, potential binding pockets were identified using computational methods for cavity detection. A series of chlorolan-1-ylium derivatives was then designed and optimized for further analysis. These compounds were subjected to molecular

docking to assess their binding affinity and interaction patterns with the target protein. Promising candidates were further evaluated using ADMET profiling to predict their pharmacokinetic behavior and toxicity risks. To examine the dynamic stability of the selected protein–ligand complexes, molecular dynamics simulations were performed under physiological conditions. Finally, density functional theory (DFT) calculations were carried out to explore the electronic characteristics and reactivity of the lead compound, supporting its suitability as a potential LAP1 inhibitor (Figure 1)

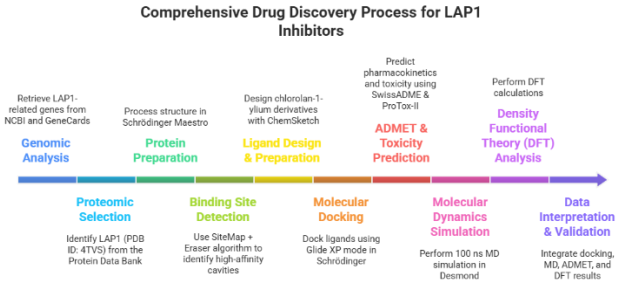

Figure 1. Computational workflow for the discovery of LAP1 inhibitors.

2.1. Genomic statistical analysis.

From the recent publications, it was found that the genes are downloaded from the NCBI database. Similarly, the gene of Lap1 was collected from recent publications it was found that Lap1 is highly expressed in skin cancer. Thus, the analysis can be done using LAP1, the gene cards, and the EMBL-EBI expression ATLAS, and the gene alterations can be analyzed with TB Tools software to generate a heatmap [14] to identify gene alteration frequency and define clusters in strings. db.org database.

2.2. Selection of proteomics.

Selection is proteomic, highly present in histology studies of skin cancer, with genes showing different alterations, and in heat map analysis. Use the software of the Protein Data Bank, AlphaFold.

2.3. LAP1 protein preparation and binding site detection.

Initially, a protein preparation algorithm within the Schrödinger Maestro_V13.8 platform was employed to prepare LAP 1 (PDB ID: 4TVS). This algorithm: hydrogen atoms were added, bond orders assigned, and protonation states adjusted to pH 7.0 ± 2.0 to mimic physiological skin microenvironment conditions, where extracellular pH variations occur due to tumor metabolism. The OPLS4 algorithm for the force field was applied. Subsequently, the eraser algorithm was utilized to select the high-affinity binding cavity and evaluate the (D-score > 1.0) for protein binding cavity [15–18].

2.4. Ligand preparation.

Using the Schrödinger Maestro platform, ligands were generated using the 2D and 3D ChemSketch Ligprep techniques, targeting a pH of 7.0 ± 2.0 after desalination. Furthermore, the tautomer generation process yielded up to 32 stereoisomers while preserving the specified chirality [19,20].

2.5. Molecular docking.

Molecular docking investigations involved establishing a grid, assessing the preparation of both the protein and ligands, and studying interactions within the specific binding cavity. Through the Schrödinger Algorithms Maestro platform, a library of 100 ligands was docked, with the top hit molecule selected based on the highest Glide Score binding affinity (kcal/mol). Maestro_V13.8 Glide XP docking mode was used to evaluate ligand binding affinities. The top-ranked chlorolan-1-ylium derivative was compared against a reference inhibitor (Vemurafenib) to benchmark performance [21–25].

2.6. ADMET and toxicity prediction.

Through the utilization of the ADME-Adsorption kinetic profile, we successfully predicted the behavioural actions of the lead compound. The open-source SwissADME program played a pivotal role in forecasting distribution, metabolism, and elimination properties by analysing pharmacokinetic data, including hydrogen bond donor and acceptor counts, molecular weight, solubility, Lipinski's Rule of Five compliance, and bioactivity scores. Additionally, assessments were conducted on organ toxicity, including the liver and immune system [26].

2.7. Molecular dynamics simulation.

Finally, the best binding hit and the protein complex stability of LAP1 (PDB ID: 4TVS) were achieved using the GPU-accelerated Desmond in Schrödinger. Using both the buffer and SPC models, the complex was resolved in an orthorhombic form. Through the system builder, the box volume was automatically adjusted based on the protein area, and the ions were recalculated accordingly. A simulation time of 100 ns was established, with a recording interval trajectory of 100 ps and an energy of 1.2. The prepared complex system was then placed into the MD workspace, resulting in the creation [27–38], which was set to 1000. The system was set to a temperature of 300 K and a pressure of 1.01325 bar, with the NPT ensemble class fixed. Before the simulation commenced, the system model underwent relaxation. Upon completion of the simulation, all interactions were thoroughly examined.

2.8. DFT orbital analysis.

The electronic properties of molecules were predicted using DFT analysis in BIOVA Materials Studio, followed by DFTB+ analysis. Prior to this, force calculations were conducted using the Forcite module after setting parameters for geometry optimization and employing the Slater-Koster library of 3ob [39]. The calculation was then initiated.

3. Results and Discussion

3.1. Genomic analysis.

The LAP protein has been examined in the Reactome pathway, specifically in its signaling through the Cancer pathway, as illustrated in Figure 2. In the context of progeria and Hutchinson-Gilford progeria syndrome (HGPS), the WNT signaling pathway is implicated, particularly in association with wild-type (WT) Lamins. This pathway directly influences the expression of cancer-associated genes such as Beta-catenin, mTOR, Notch signaling, and MAP

kinase, which are also involved in DNA damage signaling. LAP1 genes have been identified as contributors to the development of cancer cells through these pathways.

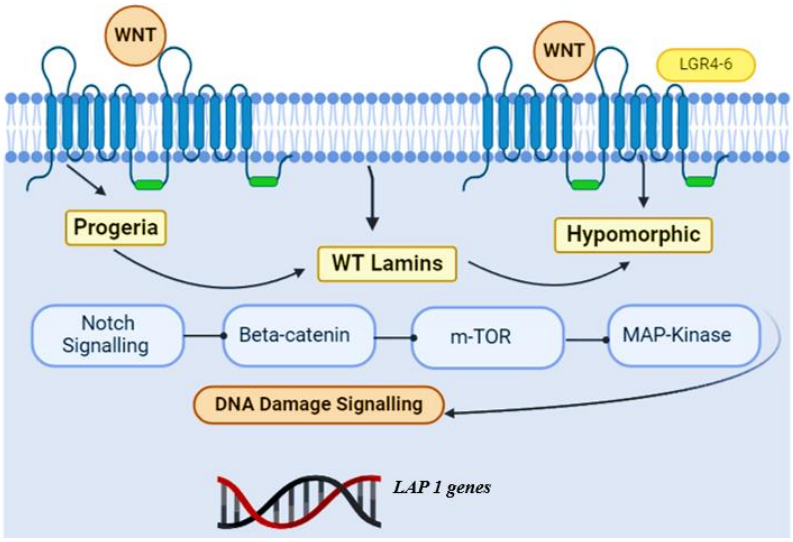

Figure 2. LAPI genes are associated with cancer signaling.

The TORIAIP1 is a subtype of the lap 1 gene, as shown in Figure 3A. The lap 1 gene, which has a very high alteration frequency, can cause irregular cell growth. The lap 1 gene was computed in AI to develop a network of statistical features for metastatic melanoma, which can predict the selection of proteomics for the development of lead invasion. The lap 1 gene has 3 subtypes classified as TORIAIPI, ANPEP, and TRAF3 [40]. It has a further 18 classified genes for each subtype. The network is shown in the heatmap of Figure 3B. The red color represents the alteration frequency of genes; the highest is MOLP-2 Genes with 110, which is responsible for metastatic melanoma [41,42]. From Figure 3C, it was found that the network cluster of LAP1 gene subtypes TORIAIP1 and TRAF3 is responsible for metastatic cell division.

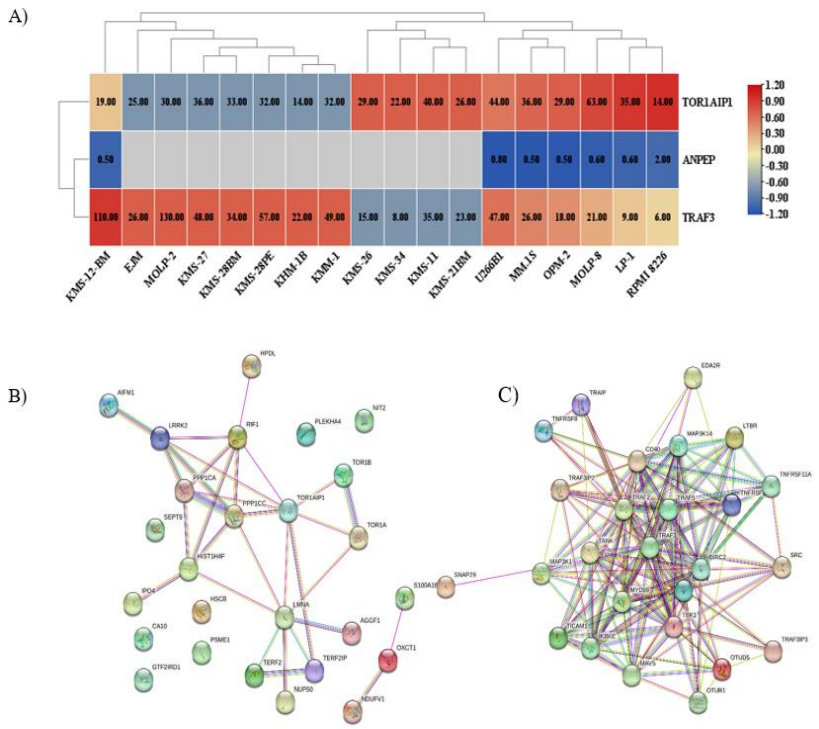

Figure 3. (A) Heatmap metastatic melanoma; **(B)** Network cluster TOR1AIP1; **(C)** Network cluster of TRAF3.

3.2. Protein preparation.

The protein was prepared using the Schrödinger Maestro interface. First, check the protein reliability for correction after viewing the Ramachandra plot mentioned in Figure 4B above.

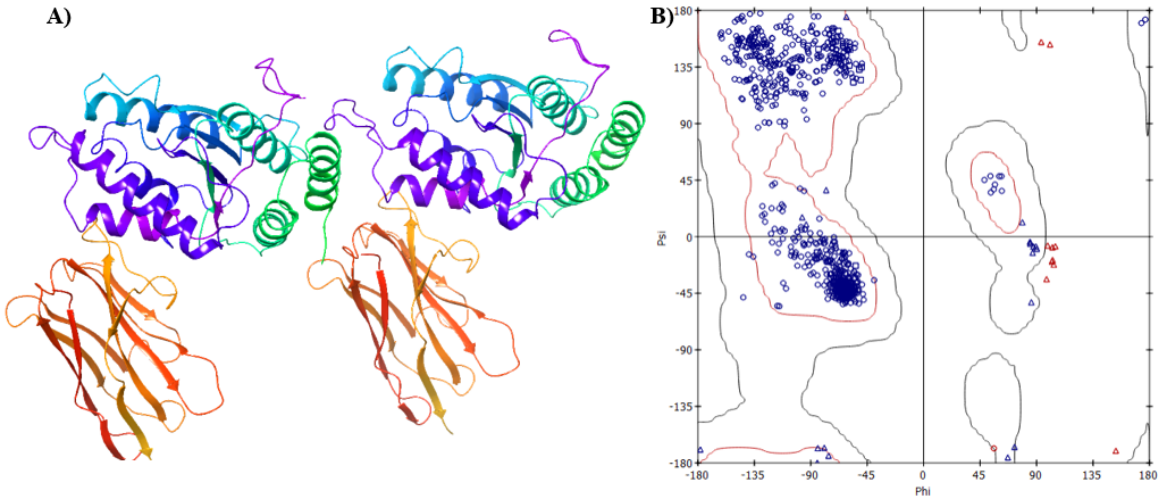

Figure 4. (A) LAP1 proteins; **(B)** Ramachandra plots.

3.3. Ligand preparation.

The pyrrole structure moiety has anticancer activity. We draw a 2D sketch in the Schrödinger Maestro interface, fuse the CL groups to the pyrrole molecule, convert chloran to the derivative, which enhances chloran activity, and generate 100 molecules to dock and confirm the best molecule.

3.4. Molecular docking.

To find possible drug binding sites based on the D-scores that are greater than 1, Maestro Schrödinger performed the X-ray crystal Lap1(pdb Id: 4TVS) using the site map detection binding cavity predicted by the Eraser algorithm, as shown in Figure 5A [43-48]. The grid generated in Schrödinger Glide within the Maestro interface corresponds to the selection entry method used to define the binding site boundaries. It was illustrated in Figure 5B X-77.574092, Y-11.395973, and Z-10.189122, respectively, with a radius of 12.851809, as shown in Figure 4B.

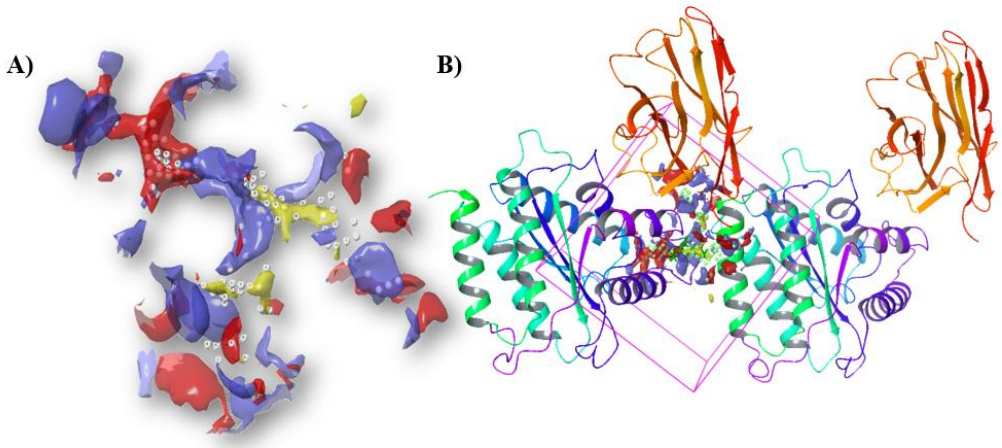

Figure 5. (A) LAP 1 binding cavity; **(B)** Grid generation on binding cavity.

The investigation into the molecular system reveals a total of 11 amino acid interactions, each playing a crucial role in defining the system's stability and specificity(Figure 6A). Notably, the system demonstrates a promising XP Glide Score of -7.456 and a calculated MMGBSA of -53.4. Among the observed interactions, hydrogen bonds are formed with TYR 549 and THR 363, while hydrophobic interactions involve PRO 546, PHE 436, ALA 364, and PRO 554. Furthermore, polar interactions are identified with SER 418, GLN 366, HIS 555, ASN 550, and SER 548, while negative charge interactions encompass GLU 367 and ASP 553, and positive charge interactions include LYS 556 and ARG 437 in the protein–ligand complex. The Cα–Cα distance map (Figure 6B) illustrates the pairwise distances between the backbone α-carbon atoms of all residues, offering a global perspective on the protein's tertiary organization. Blue regions along and near the diagonal indicate spatially close residues within secondary structural elements, whereas red and yellow areas correspond to residues that are distant in three-dimensional space. The Cβ–Cβ distance map (Panel 6C) extends this analysis to β-carbon atoms, which are part of the side chains (except in glycine), thus emphasizing side chain packing and hydrophobic core formation. The presence of contiguous blue patches here highlights regions of tight side-chain association, reflecting hydrophobic clustering or side-chain-mediated stabilizing interactions. The closest-atom distance map (Figure 6D) provides the most detailed interaction profile by calculating the minimum atomic distance between any atom of one residue and any atom of another. This representation captures not only backbone and side-chain proximity but also fine-grained non-covalent contacts, such as hydrogen bonds, salt bridges, and van der Waals interactions. The widespread distribution of blue patches across the map suggests that even residues distant in the primary sequence can engage in close atomic contacts, contributing to the overall stability of the structure.

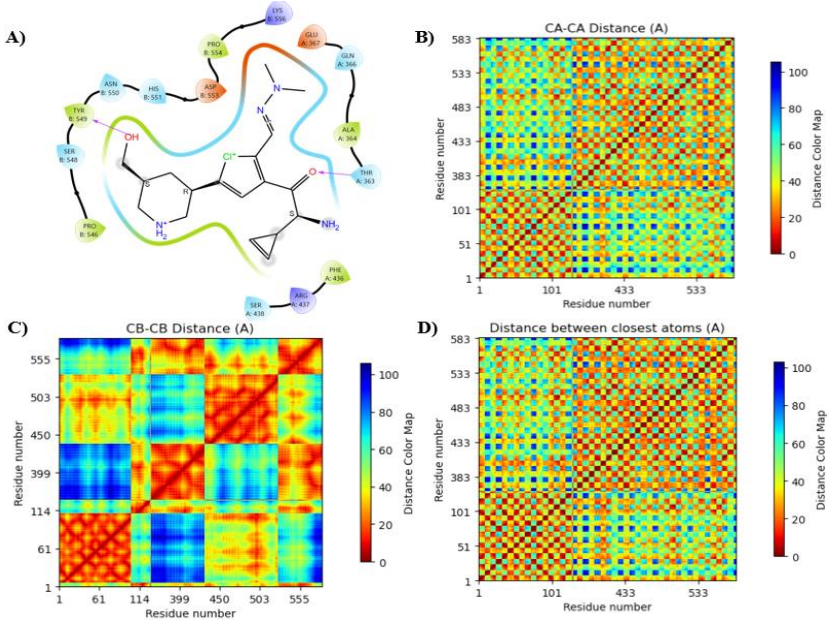

Figure 6. Lap1 active amino acid ligand interaction.(A) 2D interaction map showing key ligand–protein interactions. (B) Cα–Cα distance map of backbone residues. (C) Cβ–Cβ distance map highlighting side-chain packing. (D) Closest-atom distance map indicating detailed intermolecular contacts.

3.5. Ligand properties of the LAP1 protein surface.

Figure 4 represents the top hit docked ligand properties in the LAP 1 (Pdb ID: 4TVS) protein in a specific binding cavity of the surface. The studies revealed that the compound's ionizability was blue, indicating a basic nature, and the red color was designated as acidic

(Figure 7A). It also showed hydrogen bond donor and acceptor properties (Figure 7B). The compound has mostly aromatic edges, as illustrated in Figure 7C, and a hydrophobic nature that makes it lipid-loving. It should be most beneficial for metastatic skin cancer, as shown in Figure 7D.

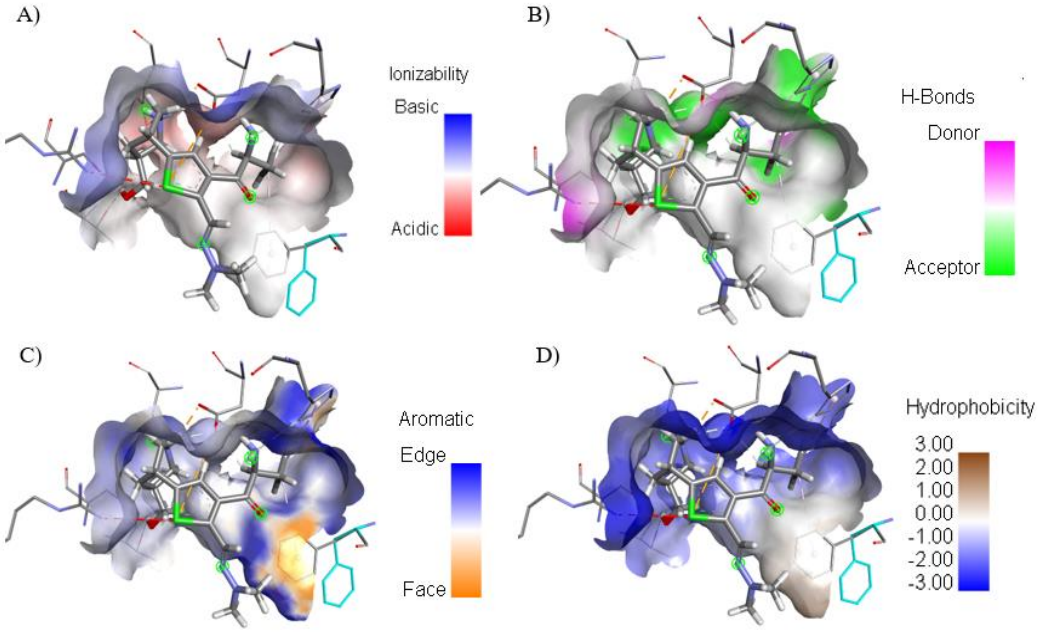

Figure 7. Protein-Ligand complex **(A)** Ionizability; **(B)** H-Bond donor and acceptor; **(C)** Aromatic; **(D)** Hydrophobicity.

3.6. ADME and toxicity prediction.

The chlorolan-1-ylium extension derivative, which was previously designed, was predicted to exhibit toxicity, including hepatotoxicity and mutagenicity, as shown in Table 2 [49-51]. The current chemotherapy drugs for melanoma have high toxicity to normal cells, but this novel chlorolan-1-ylium compound shows less toxicity and anti-tumor activity against melanoma cells.

Table 2. Prediction of physicochemical properties, toxicity, and biologically active scores.

Physiochemical properties		**Toxicity prediction**		**Bioactive score**	
Molecular Weight	375.98	Hepatotoxicity	Inactive	GPCR ligand	0.25
Rotatable bonds	8	Mutagenicity	Inactive	Ion channel	-0.10
H-bond Donor	4	Cytotoxicity	Inactive	Kinase Inhibitors	0.07
H-bond acceptor	4	Immunotoxicity	Inactive	Nuclear Receptor	-0.01
Lipid Solubility	Soluble	Androgen Receptor	Inactive	Protease inhibitors	0.37
Lipinski Rule	0	Estrogen Receptor	Inactive	Enzyme inhibitors	0.29

3.7. Molecular mechanics simulations.

Molecular docking interactions alone may not suffice to confirm the potential formation of effective hydrogen bonds. It is essential to analyse the molecular dynamics (MD) simulation, which was set up using the system builder in Desmond. It was depicted in Figure 8. In this setup, the protein was solvated using the SPC model, and the complex was established under NPT conditions at 300K. The MD simulation is poised to commence, providing a dynamic perspective on the behaviour of the system 100ns.

Stability of the Lap1 and (2R,3R,5S)-3-[(1S,2S)-2-cyclopropyl-1-hydroxypropyl]-2-[(2,2-dimethylhydrazin-1-yl)methyl]-5-[(5S)-5-(hydroxymethyl)piperidin-1-ium-3-yl]-1λ³-chlorolan-1-ylium Complex was analysed and illustrated in the Figures 9A. RMSD of Cα

started getting established from 20 ns and reached a permanent stability with some fluctuations. Figure 9B shows that the trajectory was stable up to 55 ns, and after 56 ns, it was unstable up to 100 ns. The result indicated that the Lap1 with chloran-1-yllum complex with binding interaction was stable. The MD trajectory analysed was confirmed.

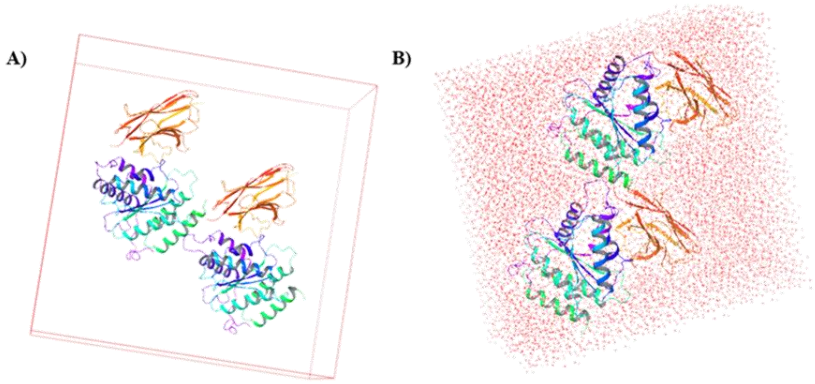

Figure 8. Solvated SPC of protein and protein complex.

AP1C–chlorolan-1-ylium complex, a 100 ns MD simulation was performed under NPT conditions. Statistical evaluation of the Cα backbone RMSD indicated a mean deviation of 2.02 ± 0.15 Å for the complex, compared to 2.48 ± 0.21 Å for the apo-protein. The trajectory stabilized after ~20 ns and maintained fluctuations within ±0.2 Å, suggesting that ligand binding contributed to enhanced structural stability.

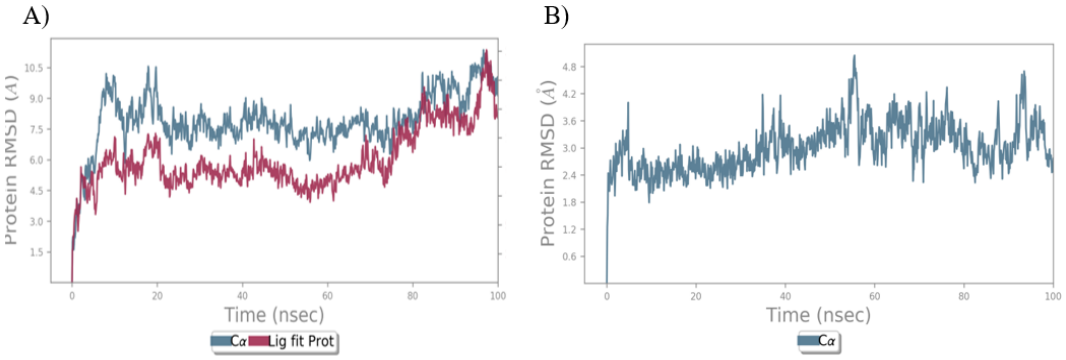

Figure 9. RMSD **(A)** Protein with chlorolan-1-ylium ligand; **(B)** LAP 1 protein.

In Figure 10B illustrates Lap1and (2R,3R,5S)-3-[(1S,2S)-2-cyclopropyl-1-hydroxypropyl]-2-[(2,2-dimethylhydrazin-1-yl)methyl]-5-[(5S)-5-(hydroxymethyl) piperidin-1-ium-3-yl]-1λ³-chlorolan-1-ylium complex the higher RMS fluctuation of amino acids observed. The Lap1 complex had less fluctuation compared to the Lap1 protein RMSF. chloran -y-ilium extension derivatives protein making stabilize the complex was found up to 4.8 Ao The LAP1 (PDB ID: 4TVS) protein (2R,3R,5S)-3-[(1S,2S)-2-cyclopropyl-1-hydroxypropyl]-2-[(2,2-dimethylhydrazin-1-yl)methyl]-5-[(5S)-5-(hydroxymethyl)piperidin-1-ium-3-yl]-1λ³-chlorolan-1-ylium Complex and interactions shown in Figure 10. fluctuation of 1.25 ± 0.09 Å across most residues, with higher flexibility (>3.5 Å) localized to solvent-exposed loop regions distant from the binding site. Critical binding site residues—TYR549, THR363, LYS556, and GLU367—exhibited minimal fluctuation (<1.0 Å), confirming the rigidity of the interaction interface.

In the conventional simulation, additional interaction cannot be found intensely. Nevertheless, the supplementary interactions can be evaluated at 100 ns and aid in ensuring the molecules are completely stable. We identified the interactions between two chains, A and B,

and the results showed that there was a high interaction at amino acid ASP_553 in the B chain and a second interaction at GLU_361 in the A chain over a 100 ns simulation period.

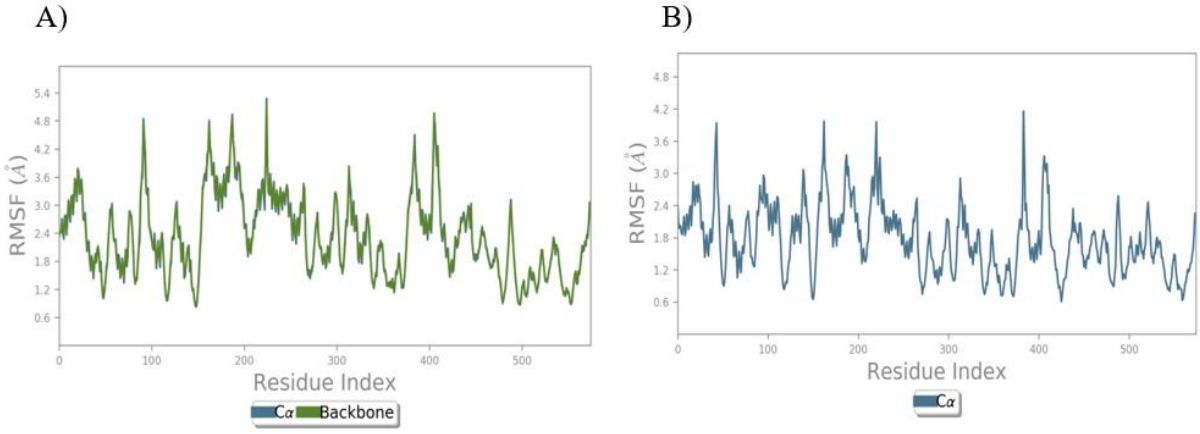

Figure 10. RMSF **(A)** Protein with chlorolan-1-ylium ligand; **(B)** LAP 1 protein.

Per-residue binding free energy decomposition identified TYR549 (–4.8 kcal/mol), LYS556 (–4.2 kcal/mol), and THR363 (–3.7 kcal/mol) as the major contributors to ligand stabilization, primarily via hydrogen bonding and π–cation interactions. Electrostatic surface mapping revealed strong charge complementarity between the positively charged chlorolan-1-ylium head group and negatively charged pockets surrounding GLU367 and ASP553.

Water bridge analysis showed that solvent-mediated hydrogen bonds between the ligand and residues SER418 and ASN550 persisted for over 70% of the simulation time, providing an additional stabilizing network within the binding cavity. The combination of stable direct hydrogen bonds, hydrophobic contacts, and persistent water bridges supports a robust ligand–protein interaction throughout the simulation period, as shown in Figure 11.

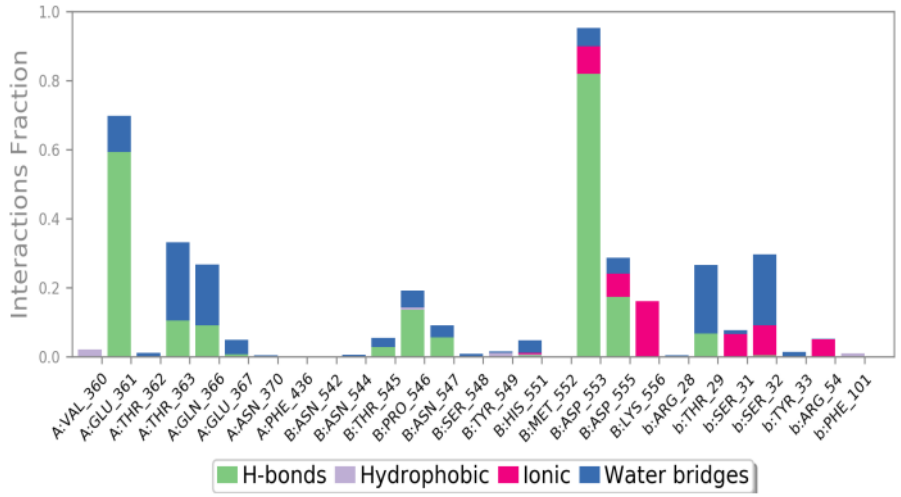

Figure 11. Chlorolan-1-yl Ligand interaction of LAP1.

The hydrophobic contacts with PHE436 and PRO546 stabilize the non-polar core within the binding site. In structural biology, such hydrophobic encapsulation can reduce the ligand's solvent exposure, lowering the entropic penalty of binding and promoting residence time—a key determinant of inhibitor potency.

3.8. DFT analysis of molecular orbitals.

The DFT analysis proved that the highest unoccupied molecular orbitals (HUMO) and lowest unoccupied molecular orbitals LUMO which define the molecular quantum mechanics.

Molecular orbitals play a vital role in the luminance chemical moiety, which provides a biological mechanism for pharmaceutical applications [52]. In Figure 12A, a grid is generated to develop a molecular orbital for chloronillum.

The aforementioned organic chloranillum chemical moiety, which provides orbital confirmation to predict the chemical hardness, chemical potential, and electrophilicity of the molecule, was identified and calculated in Figure 12 B. The HOMO energy (–0.8187 eV) was predominantly localized on the pyrrole–chlorine moiety, which is predicted to participate in π–cation and hydrogen bonding with key polar residues such as LYS556 and TYR549 in LAP1. The LUMO (–0.7850 eV) was concentrated over the heterocyclic extension, indicating regions prone to accepting electron density from protein donor groups. The calculated HOMO–LUMO gap (ΔE = 0.0337 eV)(Figure 12B), Table 3 suggests high electronic reactivity, which may facilitate efficient charge transfer during complex formation depicted in Figure 12D. extremely narrow, suggesting high chemical reactivity and the possibility of efficient charge transfer during protein–ligand complex formation. The level of theory reports a significantly larger HOMO–LUMO gap of approximately 0.092 eV (PMCID: PMC10343629). This wider gap indicates comparatively lower electronic reactivity, which may partly explain differences in binding adaptability[53]. While Vemurafenib's orbital distribution is optimized for interactions within the BRAF kinase domain, chlorolan-1-ylium's frontier orbital arrangement is more complementary to the electrostatic and structural environment of the LAP1C binding cavity.

From a biological standpoint, the reduced energy gap in chlorolan-1-ylium implies a heightened responsiveness to the polar and charged environment of the binding site. This may enhance ligand adaptability, stabilize complex formation through stronger electrostatic interactions, and facilitate persistent binding, as supported by the MD simulation results. Such a property is particularly relevant when targeting the LAP1C isoform, where inhibition is hypothesized to disrupt nuclear envelope remodeling and limit metastatic cell migration.

Table 3. Eigenvalue of orbital gaps Humo and Lumo.

Field	N	S	Eigenvalue (EV)	Type
Yes	69	+	-0.8187	HUMO
Yes	70	+	-0.7850	LUMO

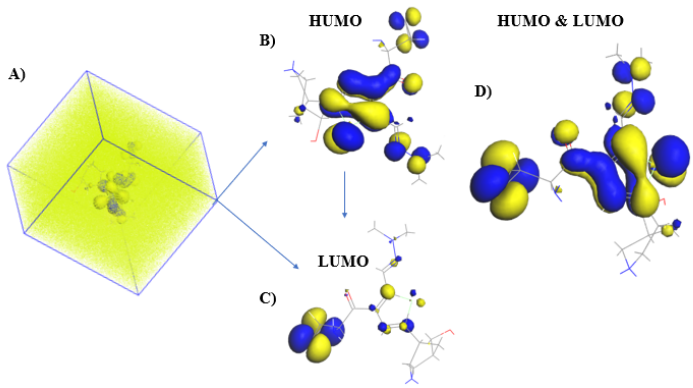

Figure 12. DFT analysis of molecular orbitals **(A)** Grid orbitals; **(B)** HUMO; **(C)** LUMO; **(D)** HUMO and LUMO

3.9. Selective binding.

The comparative docking analysis reveals that FDA-approved agents Dacarbazine, Trametinib, and Vemurafenib exhibit distinct binding interactions within the LAP1C binding

site; however, their binding affinities are notably lower than those observed for the chlorolan-1-ylium derivative in this study (Figure 13a–d). Dacarbazine (docking score: –3.121 kcal/mol; MMGBSA: –11.24 kcal/mol) primarily forms hydrogen bonds with GLU367 and polar residues such as ASN370 and GLN369, along with limited hydrophobic interactions involving PRO546 and PHE540 (Figure 13b). Trametinib (docking score: –2.400 kcal/mol) interacts through hydrogen bonds with GLU367 and ASN370, while its extended aromatic framework contributes to hydrophobic interactions with residues such as LEU557 and PRO554; however, its overall binding affinity remains comparatively weak (Figure 13c). Vemurafenib (docking score: –3.087 kcal/mol; MMGBSA: –25.06 kcal/mol) exhibits a relatively stronger hydrophobic interaction network involving LEU557, PHE540, and MET552, along with additional polar contacts with GLN369 and ASN373 (Figure 13d). The overall binding pocket and structural orientation of the protein–ligand complexes are illustrated in the ribbon representation (Figure 13a).

Despite these interactions, the electronic and structural complementarity of these reference drugs to the LAP1C binding pocket is inferior compared to the chlorolan-1-ylium derivative. The designed ligand demonstrates a more comprehensive interaction profile, including strong hydrogen bonds with TYR549 and THR363, π–cation interactions with LYS556, and hydrophobic contacts with PHE436, PRO546, and ALA364. This optimized interaction network, combined with improved docking and MMGBSA scores, suggests enhanced binding affinity and stability, supporting its potential as a selective LAP1C inhibitor.

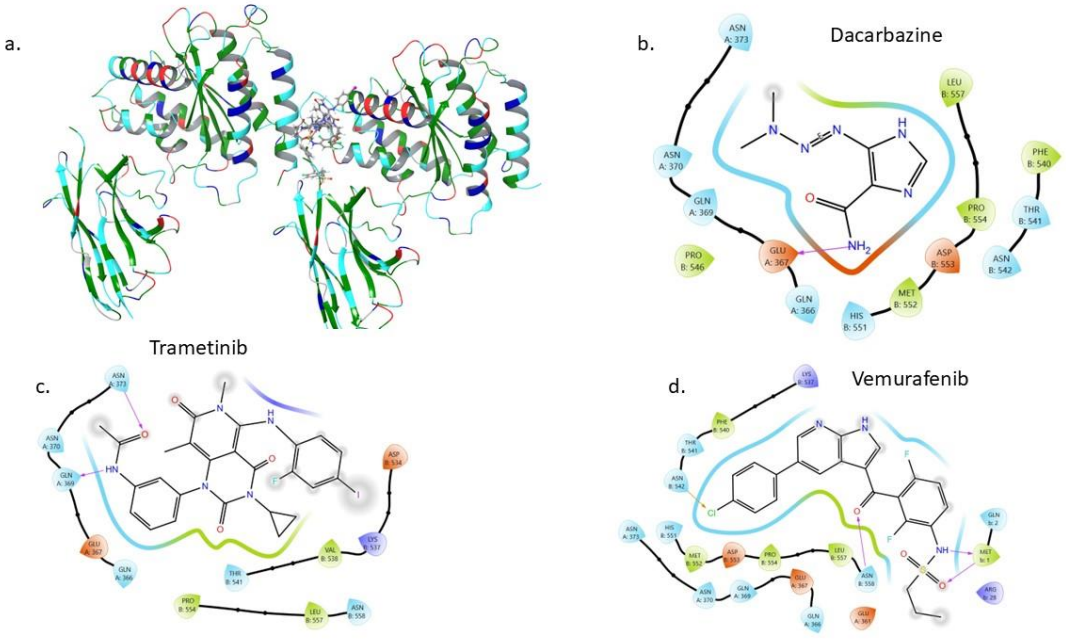

Figure 13. (a) Ribbon representation of the LAP1C protein in complex with docked ligands, showing the overall binding pocket location; **(b)** 2D interaction diagram of Dacarbazine; **(c)** 2D interaction diagram of Trametinib; **(d)** 2D interaction diagram of Vemurafenib.

4. Conclusions

This study identifies chlorolan-1-ylium derivatives as promising inhibitors of the LAP1 protein in metastatic melanoma, with strong binding affinity (–7.456 kcal/mol), favorable ADMET properties, and MD-validated stability over 100 ns. DFT analysis further supports the compound's chemical reactivity and potential biological activity. Compared with existing

therapies, this represents the first computationally validated approach to LAP1 inhibition. Nevertheless, these results are derived entirely from in silico studies, and further experimental validation is essential. Future work will focus on compound synthesis, biochemical LAP1 inhibition assays, cell-line cytotoxicity studies, and analog optimization to enhance potency and drug-likeness, thereby advancing toward preclinical evaluation.

Author Contributions

Conceptualization, I. N.; Methodology, I. N.; Software, I. N.; Formal analysis, I. N.; Writing – original draft, I. N. Supervision, M. Z. S.; Writing – review & editing, M. Z. S.; Project administration, M. Z. S. Validation, M. H.; Writing – review & editing, M. H.; Formal analysis, M. H.

Institutional Review Board Statement

Not applicable.

Informed Consent Statement

Not applicable.

Data Availability Statement

Data supporting the findings of this study are available from the corresponding author upon reasonable request.

Funding

This research received no external funding.

Acknowledgments

We acknowledge that the D3 Drug Tech lab has provided an MD simulation service.

Conflicts of Interest

The authors declare no conflict of interest.

References

1. Belote, R.L.; Le, D.; Maynard, A.; Lang, U.E.; Sinclair, A.; Lohman, B.K.; Planells-Palop, V.; Baskin, L.; Tward, A.D.; Darmanis, S.; Judson-Torres, R.L. Human melanocyte development and melanoma dedifferentiation at single-cell resolution. *Nat. Cell Biol.* **2021**, *23*, 1035-1047, https://doi.org/10.1038/s41556-021-00740-8.
2. Rabbie, R.; Ferguson, P.; Molina-Aguilar, C.; Adams, D.J.; Robles-Espinoza, C.D. Melanoma subtypes: genomic profiles, prognostic molecular markers and therapeutic possibilities. *J. Pathol.* **2019**, *247*, 539-551, https://doi.org/10.1002/path.5213.
3. Mort, R.L.; Jackson, I.J.; Patton, E.E. The melanocyte lineage in development and disease. *Development* **2015**, *142*, 620-632, https://doi.org/10.1242/dev.106567.
4. Yamaguchi, Y.; Itami, S.; Watabe, H.; Yasumoto, K.-i.; Abdel-Malek, Z.A.; Kubo, T.; Rouzaud, F.o.; Tanemura, A.; Yoshikawa, K.; Hearing, V.J. Mesenchymal–epithelial interactions in the skin : increased expression of dickkopf1 by palmoplantar fibroblasts inhibits melanocyte growth and differentiation. *J. Cell Biol.* **2004**, *165*, 275-285, https://doi.org/10.1083/jcb.200311122.

5. Hayward, N.K.; Wilmott, J.S.; Waddell, N.; Johansson, P.A.; Field, M.A.; Nones, K.; Patch, A.-M.; Kakavand, H.; Alexandrov, L.B.; Burke, H.; Jakrot, V.; Kazakoff, S.; Holmes, O.; Leonard, C.; Sabarinathan, R.; Mularoni, L.; Wood, S.; Xu, Q.; Waddell, N.; Tembe, V.; Pupo, G.M.; De Paoli-Iseppi, R.; Vilain, R.E.; Shang, P.; Lau, L.M.S.; Dagg, R.A.; Schramm, S.-J.; Pritchard, A.; Dutton-Regester, K.; Newell, F.; Fitzgerald, A.; Shang, C.A.; Grimmond, S.M.; Pickett, H.A.; Yang, J.Y.; Stretch, J.R.; Behren, A.; Kefford, R.F.; Hersey, P.; Long, G.V.; Cebon, J.; Shackleton, M.; Spillane, A.J.; Saw, R.P.M.; López-Bigas, N.; Pearson, J.V.; Thompson, J.F.; Scolyer, R.A.; Mann, G.J. Whole-genome landscapes of major melanoma subtypes. *Nature* **2017**, *545*, 175-180, https://doi.org/10.1038/nature22071.
6. Schrader, A.J. Combined chemoimmunotherapy in metastatic melanoma - is there a need for the double?. *Anti-Cancer Drugs* **2000**, *11*, 143–148, https://doi.org/10.1097/00001813-200003000-00001.
7. Legha, S.S. Treating metastatic melanoma: further considerations. *Oncology* **2009**, *23*, 500-508.
8. Scolyer, R.A.; Busam, K.J.; Barnhill, R.L. Metastatic Melanoma. In Pathology of Melanocytic Nevi and Melanoma, Barnhill, R.L., Piepkorn, M.W., Busam, K.J., Eds.; Springer Berlin Heidelberg: Berlin, Heidelberg, **2014**; pp. 529-567, https://doi.org/10.1007/978-3-642-38385-4_13.
9. Liu, M.; Yang, J.; Xu, B.; Zhang, X. Tumor metastasis: Mechanistic insights and therapeutic interventions. *MedComm* **2021**, *2*, 587-617, https://doi.org/10.1002/MCO2.100.
10. Brewer, G. LAP1 squeezes out ahead. *Nat. Rev. Cancer* **2023**, *23*, 114, https://doi.org/10.1038/s41568-023-00551-z.
11. Hipólito, A.; Martins, F.; Mendes, C.; Lopes-Coelho, F.; Serpa, J. Molecular and Metabolic Reprogramming: Pulling the Strings Toward Tumor Metastasis. *Front. Oncol.* **2021**, *11*, 656851, https://doi.org/10.3389/fonc.2021.656851.
12. Kayman Kürekçi, G.; Acar, A.C.; Dinçer, P.R. Loss of the Nuclear Envelope Protein LAP1B Disrupts the Myogenic Differentiation of Patient-Derived Fibroblasts. *Int. J. Mol. Sci.* **2022**, *23*, 13615, https://doi.org/10.3390/ijms232113615.
13. Jung-Garcia, Y.; Maiques, O.; Monger, J.; Rodriguez-Hernandez, I.; Fanshawe, B.; Domart, M.-C.; Renshaw, M.J.; Marti, R.M.; Matias-Guiu, X.; Collinson, L.M.; Sanz-Moreno, V.; Carlton, J.G. LAP1 supports nuclear adaptability during constrained melanoma cell migration and invasion. *Nat. Cell Biol.* **2023**, *25*, 108-119, https://doi.org/10.1038/S41556-022-01042-3.
14. Chen, C.; Chen, H.; Zhang, Y.; Thomas, H.R.; Frank, M.H.; He, Y.; Xia, R. TBtools: An Integrative Toolkit Developed for Interactive Analyses of Big Biological Data. *Mol. Plant* **2020**, *13*, 1194-1202, https://doi.org/10.1016/J.MOLP.2020.06.009.
15. Rasul, H.O.; Aziz, B.K.; Ghafour, D.D.; Kivrak, A. In silico molecular docking and dynamic simulation of eugenol compounds against breast cancer. *J. Mol. Model.* **2021**, *28*, 17, https://doi.org/10.1007/S00894-021-05010-W.
16. Salem, M.M.; Gerges, M.N.; Noser, A.A. Synthesis, molecular docking, and in-vitro studies of pyrimidine-2-thione derivatives as antineoplastic agents via potential RAS/PI3K/Akt/JNK inhibition in breast carcinoma cells. *Sci. Rep.* **2022**, *12*, 22146, https://doi.org/10.1038/S41598-022-26571-7.
17. Ludington, J.L. Protein Binding Site Analysis for Drug Discovery Using a Computational Fragment-Based Method. In Fragment-Based Methods in Drug Discovery, Klon, A.E., Ed.; Springer New York: New York, NY, **2015**; Volume 1289, pp. 145-154, https://doi.org/10.1007/978-1-4939-2486-8_12.
18. Ahamed, H.N.; Ismail, Y.; Navabshan, I.; Mohammed Zaidh, S.; Shanmugarajan, T.S.; Jaleel, I.; Ansari, L.H.T. Investigating the toxicity of malachite green and copper sulfate in brine shrimp: In vivo and computational study. *Toxicol. Rep.* **2024**, *13*, 101811. https://doi.org/10.1016/j.toxrep.2024.101811..
19. García-Godoy, M.J.; López-Camacho, E.; García-Nieto, J.; Nebro, A.J.; Aldana-Montes, J.F. Molecular Docking Optimization in the Context of Multi-Drug Resistant and Sensitive EGFR Mutants. *Molecules* **2016**, *21*, 1575, https://doi.org/10.3390/molecules21111575.
20. Gioia, D.; Bertazzo, M.; Recanatini, M.; Masetti, M.; Cavalli, A. Dynamic Docking: A Paradigm Shift in Computational Drug Discovery. *Molecules* **2017**, *22*, 2029, https://doi.org/10.3390/MOLECULES22112029.
21. Dash, R.; Uddin, M.M.N.; Hosen, S.M.Z.; Rahim, Z.B.; Dinar, A.M.; Kabir, M.S.H.; Sultan, R.A.; Islam, A.; Hossain, M.K. Molecular docking analysis of known flavonoids as duel COX-2 inhibitors in the context of cancer. *Bioinformation* **2015**, *11*, 543-549, https://doi.org/10.6026/97320630011543.
22. Eldehna, W.M.; El Hassab, M.A.; Elsayed, Z.M.; Al-Warhi, T.; Elkady, H.; Abo-Ashour, M.F.; Abourehab, M.A.S.; Eissa, I.H.; Abdel-Aziz, H.A. Design, synthesis, in vitro biological assessment and molecular

modeling insights for novel 3-(naphthalen-1-yl)-4,5-dihydropyrazoles as anticancer agents with potential EGFR inhibitory activity. *Sci. Rep.* **2022**, *12*, 12821, https://doi.org/10.1038/S41598-022-15050-8.
23. Das, A.P.; Agarwal, S.M. Recent advances in the area of plant-based anti-cancer drug discovery using computational approaches. *Mol. Divers.* **2024**, *28*, 901-925, https://doi.org/10.1007/S11030-022-10590-7.
24. Yang, W.; Soares, J.; Greninger, P.; Edelman, E.J.; Lightfoot, H.; Forbes, S.; Bindal, N.; Beare, D.; Smith, J.A.; Thompson, I.R.; Ramaswamy, S.; Futreal, P.A.; Haber, D.A.; Stratton, M.R.; Benes, C.; McDermott, U.; Garnett, M.J. Genomics of Drug Sensitivity in Cancer (GDSC): a resource for therapeutic biomarker discovery in cancer cells. *Nucleic Acids Res.* **2013**, *41*, D955-D961, https://doi.org/10.1093/nar/gks1111.
25. Habeeb, M.; Woon You, H.; Balasaheb Aher, K.; Balasaheb Bhavar, G.; Suryabhan Pawar, S.; Dnyaneshwar Gaikwad, S. Artificial neural networks for the prediction of mechanical properties of CGNP/PLGA nanocomposites. *Mater. Today Proc.* **2023**, https://doi.org/10.1016/j.matpr.2023.08.354.
26. Alam, S.; Khan, F. Virtual screening, Docking, ADMET and System Pharmacology studies on Garcinia caged Xanthone derivatives for Anticancer activity. *Sci. Rep.* **2018**, *8*, 5524, https://doi.org/10.1038/S41598-018-23768-7.
27. Hospital, A.; Goñi, J.R.; Orozco, M.; Gelpí, J.L. Molecular dynamics simulations: advances and applications. *Adv. Appl. Bioinform. Chem.* **2015**, *8*, 37-47, https://doi.org/10.2147/AABC.S70333.
28. Shukla, R.; Tripathi, T. Molecular Dynamics Simulation of Protein and Protein–Ligand Complexes. In Computer-Aided Drug Design, Singh, D.B., Ed.; Springer Singapore: Singapore, **2020**; pp. 133-161, https://doi.org/10.1007/978-981-15-6815-2_7.
29. Singh, D.B. Computer-Aided Drug Design. Springer Singapore: Singapore, **2020**, https://doi.org/10.1007/978-981-15-6815-2.
30. Priya, R.M.; Irfan, N.; Mohammed Zaidh, S. Binding and dynamics of diferuloylmethane-pyrimidine with C-Met protein. *J. Indian Chem. Soc.* **2025**, *102*, 101849, https://doi.org/10.1016/j.jics.2025.101849
31. Fuzo, C.A.; Degrève, L. Effect of the thermostat in the molecular dynamics simulation on the folding of the model protein chignolin. *J. Mol. Model.* **2012**, *18*, 2785-2794, https://doi.org/10.1007/S00894-011-1282-2.
32. Barducci, A.; Bonomi, M.; Parrinello, M. Metadynamics. *Wiley Comput. Mol. Sci.* **2011**, *1*, 826-843, https://doi.org/10.1002/WCMS.31.
33. Paquet, E.; Viktor, H.L. Molecular Dynamics, Monte Carlo Simulations, and Langevin Dynamics: A Computational Review. *BioMed Res. Int.* **2015**, *2015*, 183918, https://doi.org/10.1155/2015/183918.
34. Irfan, N.; Vaithyanathan, P.; Anandaram, H.; Mohammed Zaidh, S.; Priya Varshini, S.; Puratchikody, A. Active and allosteric site binding MM-QM studies of Methylidene tetracyclo derivative in PCSK9 protein intended to make a safe antilipidemic agent. *J. Biomol. Struct. Dyn.* **2024**, *42*, 6813-6822, https://doi.org/10.1080/07391102.2023.2239928.
35. Zaidh, S.M.; Vengateswaran, H.T.; Habeeb, M.; *et al.* Network pharmacology and AI in cancer research uncovering biomarkers and therapeutic targets for RALGDS mutations. *Sci. Rep.* **2025**, *15*, 10938, https://doi.org/10.1038/s41598-025-91568-.
36. Mohammed Zaidh, S.; Aher, K.B.; Bhavar, G.B.; Irfan, N.; Ahmed, H.N.; Ismail, Y. Genes adaptability and NOL6 protein inhibition studies of fabricated flavan-3-ols lead skeleton intended to treat breast carcinoma. *Int. J. Biol. Macromol.* **2024**, *258*, 127661, https://doi.org/10.1016/j.ijbiomac.2023.127661.
37. Habeeb, M.; Deepthi, K.L.; Prasad, M.V.V.; Irfan, N.; Ali, S.L.; Navyaja, K. Development characterization and molecular simulation studies of metoclopramide HCl and tramadol HCl bilayer tablets. *Res. J. Pharm. Technol.* **2022**, *15*, 529-534, https://doi.org/10.52711/0974-360X.2022.00085.
38. Habeeb, M.; You, H.W.; Umapathi, M.; Ravikumar, K.K.; Hariyadi; Mishra, S. Strategies of Artificial intelligence tools in the domain of nanomedicine. *J. Drug Deliv. Sci. Technol.* **2024**, *91*, 105157, https://doi.org/10.1016/j.jddst.2023.105157.
39. Weller, J.A.; Rohs, R. Structure-Based Drug Design with a Deep Hierarchical Generative Model. *J. Chem. Inf. Model.* **2024**, *64*, 6450-6463, https://doi.org/10.1021/acs.jcim.4c01193.
40. Akbarzadeh, S.; Coşkun, Ö.; Günçer, B. Studying protein–protein interactions: Latest and most popular approaches. *J. Struct. Biol.* **2024**, *216*, 108118, https://doi.org/10.1016/j.jsb.2024.108118.
41. Nourbakhsh, M.; Degn, K.; Saksager, A.; Tiberti, M.; Papaleo, E. Prediction of cancer driver genes and mutations: the potential of integrative computational frameworks. *Brief. Bioinform.* **2024**, *25*, bbad519, https://doi.org/10.1093/bib/bbad519.
42. Cornilescu, G.; Bindu, L.; Sternicki, L.; Chao, F.-A.; Gillette, W.K.; Fer, N.; Colombus, J.; Castillo, J.; Bonilla, P.A.; Van, Q.N.; Larsen, E.; Hong, M.; Burgan, W.; Turbyville, T.; Nissley, D.V.; Liu, M.; Quinn,

R.; Jean-Francois, F.L. Natural Product Graveoline Modulates Kirsten Rat Sarcoma Viral Oncogene Homologue (KRAS) Membrane Association: Insights from Advanced Spectroscopic Studies. *ACS Pharmacol. Transl. Sci.* **2024**, *7*, 1983-1995, https://doi.org/10.1021/acsptsci.4c00075.

43. Myung, Y.; de Sá, A.G.C.; Ascher, D.B. Deep-PK: deep learning for small molecule pharmacokinetic and toxicity prediction. *Nucleic Acids Res.* **2024**, *52*, W469-W475, https://doi.org/10.1093/nar/gkae254.
44. Liu, J.; Zhang, Y.; Yi, C.; Zhang, R.; Yang, S.; Liu, T.; Jia, D.; Yang, Q.; Peng, S. Evaluation of Antioxidant Properties and Molecular Design of Lubricant Antioxidants Based on QSPR Model. *Lubricants* **2024**, *12*, 3, https://doi.org/10.3390/LUBRICANTS12010003.
45. Luo, Y.; Chen, H.; Huang, C.; He, S.; Wen, Q.; Cai, D. Structure Elucidation of a Novel Polysaccharide Isolated from *Euonymus fortunei* and Establishing Its Antioxidant and Anticancer Properties. *Int. J. Anal. Chem.* **2024**, *2024*, 8871600, https://doi.org/10.1155/2024/8871600.
46. Islam, M.R.; Islam Sovon, M.S.; Amena, U.; Rahman, M.; Hosen, M.E.; Kumer, A.; Bourhia, M.; Bin Jardan, Y.A.; Ibenmoussa, S.; Wondmie, G.F. Ligand-based drug design against Herpes Simplex Virus-1 capsid protein by modification of limonene through in silico approaches. *Sci. Rep.* **2024**, *14*, 9828, https://doi.org/10.1038/S41598-024-59577-4.
47. Bibi, S.; Urrehaman, S.; Akram, M.; Amin, R.; Majeed, H.; Khan, S.R.; Younis, S.; Bai, F.-Q. Molecular docking and DFT study of antiproliferative ribofuranose nucleoside derivatives targeting EGFR and VEGFR2in cancer cells. *Comput. Biol. Chem.* **2024**, *113*, 108187, https://doi.org/10.1016/j.compbiolchem.2024.108187.
48. Ramadan, S.K.; Abd-Rabboh, H.S.M.; Abdel Hafez, A.A.; Abou-Elmagd, W.S.I. Some pyrimidohexahydroquinoline candidates: synthesis, DFT, cytotoxic activity evaluation, molecular docking, and *in silico* studies. *RSC Adv.* **2024**, *14*, 16584-16599, https://doi.org/10.1039/D4RA02271H.
49. Ahmad, S.; Ali, S.S.; Iqbal, A.; Ali, S.; Hussain, Z.; Khan, I.; Khan, H. Using a dual immunoinformatics and bioinformatics approach to design a novel and effective multi-epitope vaccine against human torovirus disease. *Comput. Biol. Chem.* **2024**, *113*, 108213, https://doi.org/10.1016/j.compbiolchem.2024.108213.
50. Wilson, J.; Sokhansanj, B.A.; Chong, W.C.; Chandraghatgi, R.; Rosen, G.L.; Ji, H.-F. Fragment databases from screened ligands for drug discovery (FDSL-DD). *J. Mol. Graph. Model.* **2024**, *127*, 108669, https://doi.org/10.1016/j.jmgm.2023.108669.
51. El Rhabori, S.; El Aissouq, A.; Daoui, O.; Elkhattabi, S.; Chtita, S.; Khalil, F. Design of new molecules against cervical cancer using DFT, theoretical spectroscopy, 2D/3D-QSAR, molecular docking, pharmacophore and ADMET investigations. *Heliyon* **2024**, *10*, e24551, https://doi.org/10.1016/j.heliyon.2024.e24551.
52. Priya, R.M.; Zaidh, S.M.; Navabshan, I.; Venkataraman, S.; Ahmed, H.N.; Ismail, Y. Pharmacophore-based SAR Analysis and Synthetic Route Review of Imidazole Core Analogues. *Curr. Appl. Sci. Technol.* **2024**, *25*, e0261082, https://doi.org/10.55003/cast.2024.261082.
53. Grodner, B.; Żołek, T.; Kutner, A. Nonaqueous capillary electrophoretic separation of analogs of (24R)-1,24-dihydroxyvitamin D3 derivative as predicted by quantum chemical calculations. *Molecules* **2023**, *28*, 5055. https://doi.org/10.3390/molecules28135055.

Publisher's Note & Disclaimer